Selective sensitization strategy for high-performance panchromatic dye-sensitized solar cells incorporated with ruthenium-based double dyes

Eun Ji Cho [a,1], Jung Keun Cha [a,1], Guiming Fu [a,1], Hyun Soo Cho [a], Hyung Woo Lee [a,b,c], Soo Hyung Kim [a,b,c,*]

[a] Department of Nanofusion Technology, Pusan National University, 2, Busandaehak-ro 63beon-gil, Geumjeong-gu, Busan 46241, Republic of Korea
[b] Department of Nanoenergy Engineering, Pusan National University, 2, Busandaehak-ro 63beon-gil, Geumjeong-gu, Busan 46241, Republic of Korea
[c] Research Center for Energy Convergence Technology, Pusan National University, 2, Busandaehak-ro 63beon-gil, Geumjeong-gu, Busan 46241, Republic of Korea

ABSTRACT

To facilitate the assembly of high-performance panchromatic dye-sensitized solar cells (DSSCs), it is important to determine the selection and sensitization of dyes in photoelectrodes. This paper reports the fabrication of panchromatic DSSCs comprising freestanding and fixed TiO$_2$ thin films (TFs). These TFs constitute a bilayered photoelectrode coated with ruthenium-based double dyes. In addition, we systematically examine the effect of the separated sensitization of double dyes on DSSC performance. The UV–vis spectroscope measurements reveal that the ruthenium-based dyes exhibit light-absorbance values in the order of C106 > N719 > N749. The results of the separated sensitization of C106 (bottom layer)/ N719 (top layer) dyes reveal a maximum efficiency of 8.10 %. Correspondingly, the separated sensitization of N749/N719 dyes yields a poor PCE of 5.85 %. In addition, the mixed sensitization of the double dyes (i.e., C106 + N719, C106 + N749, and N719 + N749) is found to demonstrate poor DSSC performance compared to the corresponding separated sensitization (i.e., C016/N719, C106/N749, and N719/N749). This can be attributed to the occurrence of negative interactions between mixed dyes. Therefore, to improve the panchromatic DSSC performance, it is suggested that dyes with high and low light-absorbance values be sensitized on the bottom and top layers, respectively.

© 2022 The Korean Society of Industrial and Engineering Chemistry. Published by Elsevier B.V. All rights reserved.

Introduction

Globally, fossil fuels constitute the main source of energy. However, the use of fossil fuels increases carbon-dioxide emissions, which eventually result in global warming and environmental pollution. To overcome these problems, energy-conversion devices based on the use of renewable energy sources have witnessed increased demands recently. Solar cells are considered promising energy-conversion devices that efficiently transform light energy into electric energy. Among the different types of solar cells, those of the dye-sensitized variety (DSSCs) have been developed to afford users the advantages of simple and affordable manufacturing process, transparent and diverse colors-based applicability, high efficiency, and low production cost [1–5].

In general, DSSCs comprise several parts—dye-sensitized semiconductor oxide (e.g., TiO$_2$) thin-film-coated conducting substrate-based photoelectrode, iodide/triiodide-based liquid electrolyte, and Pt-coated conducting substrate-based counter electrode. The irradiation of dye molecules by sunlight results in the generation of electrons through photoexcitation. Subsequently, these electrons are introduced into the semiconductor oxide and reach the conducting photoelectrode. Thereafter, the photogenerated electrons finally reach the counter electrode, wherein the DSSC current cycle is completed by their entering into the liquid electrolyte [6–10].

Among the different DSSC components and processes, the type selection and sensitization of dyes are important owing to their significant effect of the resulting DSSCs performance. The ruthenium (Ru) (II)-based dyes are typically used in DSSCs because they exhibit a wide yet stable light-absorption range between the near ultraviolet (UV) and near infrared (IR) regions of the electromagnetic spectrum. These Ru(II)-based dyes are often used in combination with TiO$_2$ nanoparticle (NP)-accumulated thin films (TFs) in the DSSC photoelectrode [11–13]. Generally, because a single dye type is often used in DSSCs, the amount of energy harvested could

be limited. Therefore, the mixed-sensitization of different dyes coated on TiO_2 TFs in the DSSC photoelectrode has been extensively investigated to increase the amount of solar-energy harvesting [14–16]. During the mixed-sensitization process, the TiO_2 TF-based photoelectrode is simply immersed into a multiple-dye-dispersed solution. The resulting multiple-dye-sensitized TiO_2 TFs are expected to increase the wavelength (or frequency) range of light absorbance. However, the mixed-sensitization of multiple dyes could cast an adverse effect on improving the light harvesting owing to the occurrence of negative interactions. In these adverse interactions, the transport of the electrons generated by certain dye molecules can be shunt by another type of neighboring dye molecule owing to the difference between energy levels. This could interfere with increasing the current density of DSSCs [17–20].

To overcome this shortcoming of the mixed-sensitization process, several researchers have attempted to realize the dye-sensitization of TiO_2 TFs by sequentially immersing them into different dye solutions [21–23]. However, these previous approaches have been unable to produce stable TiO_2 TFs incorporated with separated dyes. This failure could be attributed to the complicated experimental conditions—dye concentration and coating duration—and unavoidable contamination of dye solutions with different dye types. This paper reports the fabrication of separate freestanding and fixed TiO_2 TFs, which are separately incorporated with different dyes that demonstrate high extinction coefficients in specific wavelength ranges. Three commercially available Ru(II)-based dyes—N719, N749, and C106—are selectively applied to the bilayered TiO_2 TFs to examine the effect of the separated and mixed positioning of double dyes on DSSC performance.

Experimental procedure

Fabrication of TiO_2 TFs and DSSC assembly

Fig. 1 depicts the steps performed in this study for TiO_2 TF fabrication. To this end, glass deposited with fluorine-doped tin oxide (FTO, SnO_2:F) was first cleaned via ultrasonic treatment using ethanol, acetone, and deionized water. Thereafter, the FTO-coated glass was dipped in a $TiOCl_2$-dispersed (i.e., $TiOCl_2$ (0.247 mL) + deionized water (20 mL)) aqueous solution (70 °C & 0.5 h). Subsequently, the FTO-coated glass was removed from the solution in a closed furnace (500 °C & 0.5 h). As a second step, we prepared a TiO_2 NP-based paste, which was uniformly mixed with TiO_2 NPs (0.3 g; P25, Degussa), acetic acid (0.05 mL; Sigma-Aldrich), terpineol (1 g; Sigma-Aldrich), and ethanol (3 mL) in a vial using a ultrasonicator operated at 750 W and 40 Hz for 1 h. Meanwhile, ethyl cellulose (0.15 g; Sigma-Aldrich) and ethanol (5 mL) were similarly sonicated in a vial. The prepared solutions were subsequently mixed to obtain the TiO_2 paste via thermal removal of ethanol. Thereafter, the screen-printing process was performed to prepare TiO_2 TFs on the pretreated FTO glass. This comprised a 20-μm-thick bottom layer with a photoactive area of 0.16 cm^2. Upon completion of the sintering process in a closed furnace (500 °C & 0.5 h), the TiO_2 TFs were immersed in a 30 mM dye solution for 24 h to facilitate dye adsorption. Meanwhile, the freestanding TiO_2 TF was prepared by depositing a photoresist on the fluorine-free side of FTO glass using a two-step spin-coating process. The first and second steps of the spin-coating process involved rotations at 500 and 4000 rpm for 10 and 30 s, respectively. Subsequently, a screen-printed TiO_2 TF was formed on the photoresist-coated FTO glass. Thereafter, the former was easily separated from the FTO glass by removing the photoresist layer by immersing the sample in a developer solution. After removal of the photoresist residue with deionized water, the freestanding TiO_2 TF was sintered in a closed furnace (500 °C & 0.5 h). This

was followed by sensitization in a dye-dispersed aqueous solution for 24 h. Finally, the fixed (bottom) and freestanding (top) TiO_2 TF layers were combined using a mounting press machine (DS2-500 N, IMADA; Japan) operated under 128-N applied load.

To fabricate the counter electrode, Pt-coated FTO glass substrate was prepared using an ion-sputtering machine (E1010, Hitachi; Japan). A hollow rectangular-structured polymer sheet (Surlyn, DuPont; USA) of thickness 120 μm was placed between both electrodes and heated at 100 °C for 1 min. Subsequently, the iodide electrolyte (AN-50, Solaronix, SA; Switzerland) was supplied and sealed with the hot, molten polymer to complete the DSSC assembly.

Characterization of TiO_2 NPs and dye adsorption

In this study, the characterization of TiO_2 NPs was performed using field-emission scanning-electron microscopy (FE-SEM; SUPRA25, ZEISS; Germany) at 15 kV, field-emission transmission-electron microscopy (FE-TEM; JEM-2100F, JEOL; Japan) at 200 kV, and X-ray diffraction (XRD; Xpert3, Malvern Panalytical; UK) involving Cu Kα radiations. As already mentioned, three different dyes—N719 ($C_{58}H_{86}N_8O_8RuS_2$; Solaronix; Switzerland), N749 ($C_{69}H_{117}N_9O_6 RuS_3$; Solaronix; Switzerland), and C106 ($C_{44}H_{44}N_6O_4RuS_6$; Solaronix; Switzerland)—were used in this study, and their chemical structures are depicted in Fig. 2.

To determine the adsorbed amount of dye, the dye-coated TiO_2 TFs were dipped into a NaOH solution (0.1 mol·L^{-1}) for dissolving the dyes. The resulting dye-dissolved solution was analyzed using UV–Vis spectrometry (Cary 5000, Agilent; USA).

DSSC performance evaluation

In this study, DSSC performance was examined using a solar simulator (PEC-L11, Peccell Technologies, Inc.; Kanagawa, Japan) operated at 1.5 air mass and 1 sun. With the assistance of Keithley SMU 2400 source meter (Cleveland, USA), the current–density–voltage (J–V) curves and electrochemical impedance spectra (EIS) were measured. To this end, we considered the 0.1–100-kHz frequency range along with 10-mV open voltage amplitude. Moreover, with the assistance of another solar simulator (PEC-S20, Peccell Technologies, Inc.; Kanagawa, Japan) along with an arc lamp (LS-150-Xe, Abet Technologies Inc.), we measured the incident photon–electron conversion efficiency (IPCE) in the 300–900-nm wavelength range.

Results and discussion

In this study, we performed the SEM and TEM analyses to observe the particle-size distribution and structure of TiO_2. As observed, the average primary size of the TiO_2 NPs equaled 25.51 nm, and their structures were predominantly spherical. The sintering of TiO_2 NPs in a closed furnace resulted in the creation of several pores owing to the thermal removal of the ethyl-cellulose templates (Fig. 3(a) and 3(b)). In addition, the heating process caused the primary TiO_2 NPs to be partially sintered, as depicted in Fig. 3(c). The cross-sectional SEM image (Fig. 3(d)) reveals the TiO_2 NPs to remain tightly accumulated in the fixed-bottom and freestanding-top TiO_2 TFs owing to the compaction process (Fig. 1). The total thickness of the TiO_2 NP-accumulated TFs equaled 55.57 μm.

Furthermore, XRD analysis was performed in this study to examine the crystallinity and crystal structures of TiO_2 NPs after completion of the sintering process. The results of this analysis are depicted in Fig. 4. The strong peaks corresponding to the anatase ($2\theta = 25.26°$) and rutile ($2\theta = 27.35°$) phases are clearly visible
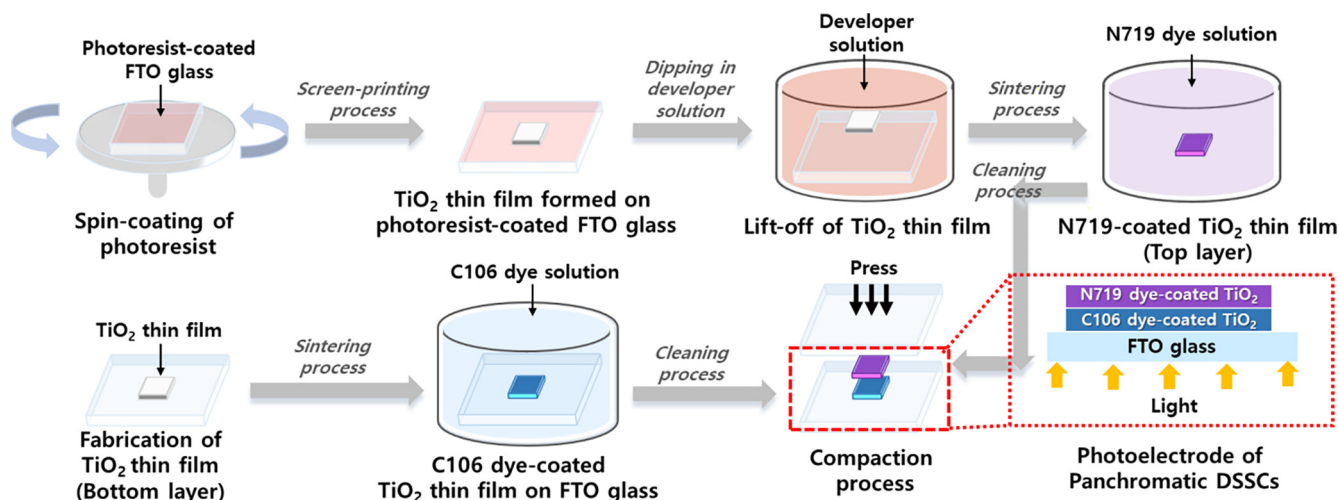
Fig. 1. Schematic of steps involved in fabrication of panchromatic DSSCs selectively sensitized with double dyes in bilayered TiO₂ TF-based photoelectrode.
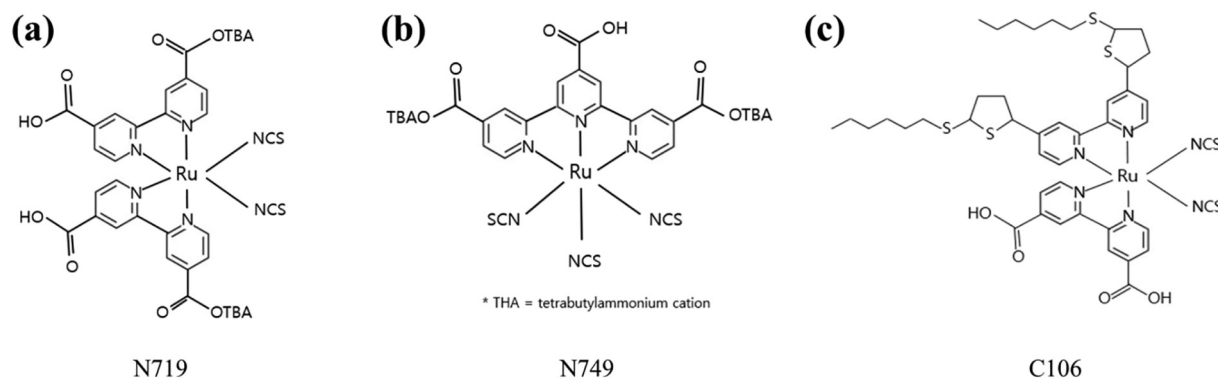

Fig. 2. Chemical structures of (a) N719, (b) N749, and (b) C106 dye molecules.

and do not contain any impurities. The calculated crystallite size of anatase and rutile using Scherrer's equation was 19.8 nm and 28.7 nm, respectively [24]. In addition, the calculated phase compositions for anatase and rutile using Spurrand Myers's equation was 79.89 % and 19.90 %, respectively [25].

Fig. 5 presents the results of the UV–vis spectroscopy measurements to examine the light-absorbance characteristics of the different dyes—N719, N749, and C106—considered in this study. As can be seen, the N719 dye demonstrates strong peaks at wavelengths of 312, 388, and 531 nm while the corresponding peaks for N749 appear at 325, 413, and 615 nm. The C106 dye demonstrates strong peaks at 312, 351, and 540 nm. Moreover, the UV–vis spectra demonstrate multiple peaks in the visible-light wavelength range. The first peak represents a $\pi–\pi^*$ electron transition while the second and third peaks represent the metal-to-ligand charge transfer transitions [26–28]. The molar extinction coefficient was calculated in the 300–900-nm wavelength range using the Lambert–Beer law. This law is given by $A = \varepsilon\,c\,l$, where A, ε, c, and l denote the light absorbance, molar extinction coefficient ($M^{-1} \cdot cm^{-1}$), molar concentration (M), and thickness (cm) of the solution through which the incident light passes. As observed in this study, the values of the major extinction coefficients for N719, N749, and C106 equal $1.45 \times 10^4\ M^{-1}\ mol^{-1}$ at 531 nm, $0.86 \times 10^4\ M^{-1}\ mol^{-1}$ at 615 nm, and $1.76 \times 10^4\ M^{-1}\ mol^{-1}$ at 540 nm, respectively. Moreover, the light-absorbance property of these can be rated in the order C106 > N719 > N749. Interestingly, all mixed double-dye pairs (i.e., N719 + N749, C106 + N719,

C106 + N749) demonstrated only moderate light absorbance across the wavelength range considered in this study.

To examine the effect of double-dye selection and sensitization on the DSSC performance, the three Ru(II)-based dyes were selectively applied to the bilayered TiO₂ photoelectrodes. Therefore, panchromatic DSSCs of different configurations were fabricated to investigate their performance as well as the effect of varying the dye-sensitization sequence in the TiO₂ photoelectrodes. The results of this analysis are presented in Table 1. In addition, the performances of the single and mixed double dye-sensitized solar cells (i.e., S-DSSCs and D-DSSCs) were compared. As can be observed, among the S-DSSC cases, the C106-based S-DSSC exhibited a power conversion efficiency (PCE) value of 7.52 %, which exceeds those of its N719- and N749-based counterparts (i.e., 7.06 % and 6.21 %). This is because the C106 dye demonstrates better light absorbance compared to N719 and N749 dyes (Fig. 5). Among the D-DSSC cases, the observed PCE equaled 5.85 % when the bilayered TiO₂ TFs adsorbed the N749 and N719 dyes on the bottom and top layer, respectively. However, replacing the bottom-layer dye with C106 revealed a significant increase in PCE to 8.10 %. Therefore, it can be inferred that the values of the short-circuit current density (J_{sc}) and PCE increase significantly when the bottom and top TiO₂ TFs are coated with dyes (i.e., C106 and N719/N749) that exhibit wide and narrow absorbance wavelength ranges as well as high and low molar extinction coefficients, respectively. This confirms that dyes with high molar
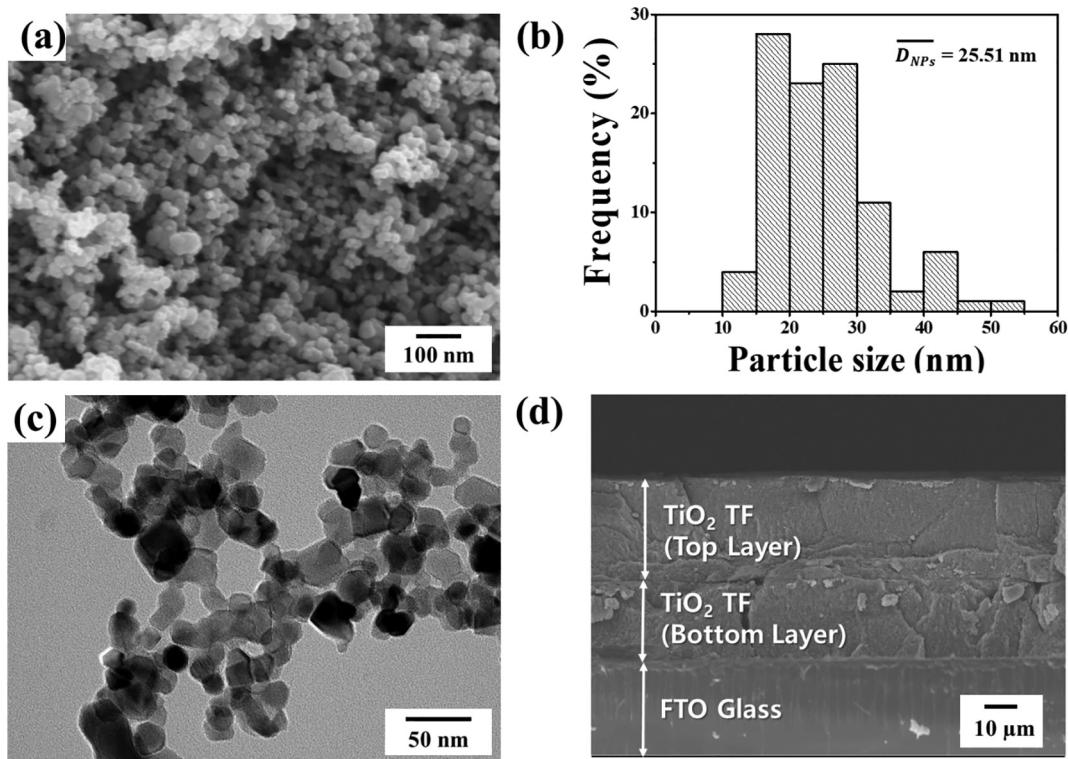
Fig. 3. (a) SEM image and (b) particle-size distribution of TiO$_2$ NPs ($\overline{D_{NPs}}$ denotes the average primary size of TiO$_2$ NPs), (c) TEM image of TiO$_2$ NPs, and (d) cross-sectional SEM image of TiO$_2$ TFs formed on FTO glass substrate.
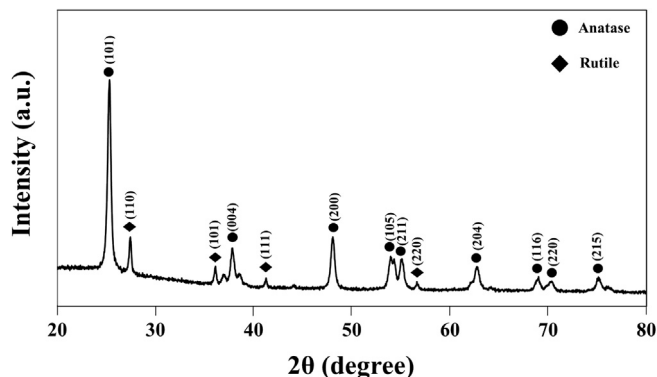

Fig. 4. Results of XRD analysis of TiO$_2$ NPs.

extinction coefficients must be placed underneath to increase the PCE value of panchromatic DSSCs.

Fig. 6 depicts the performance of panchromatic DSSCs, which are selectively sensitized with double dyes that exhibit high and low molar extinction coefficients in their bottom and top layers, respectively. The cases corresponding to mixed double dyes are also presented for comparison. As can be seen, the separated sensitization improves the values of both J$_{sc}$ and PCE in the order C106/N719 > C106/N749 > N719/N749. However, these values remain similar or even deteriorate when mixed sensitization is performed (Table 1 and Fig. 6(a)). Fig. 6(b) shows the Nyquist plots, which contain information about the resistances at the various interfaces in DSSCs. The Nyquist plot typically depicts three arcs with respect to frequency, and the resistance is calculated in terms of the width of the arcs in the real axis. The first, second, and third arcs represent the resistance across the electrolyte–counter-electrode interface, resistance (R$_{rec}$) across TiO$_2$–dye–electrolyte inter-
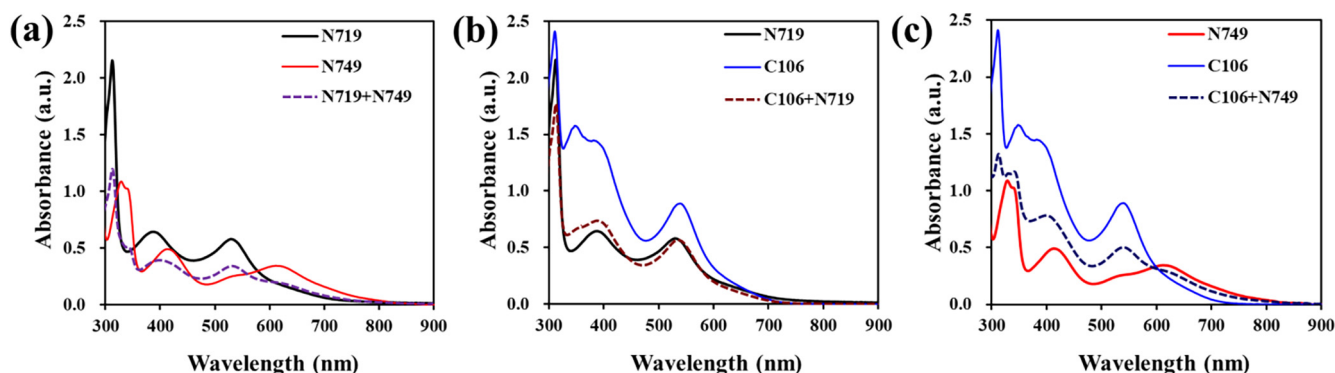

Fig. 5. UV–vis spectra of different dyes in ethanol (40 μM): (a) N719, N749, N719 + N749, (b) N719, C106, N719 + C106, and (c) N749, C106, N749 + C106.

Table 1

Summary of photovoltaic performances of different S-DSSC and D-DSSC configurations selectively sensitized using the N719, N749, and C106 dyes.

Sensitization type	Arrays of dye adsorbed on TiO$_2$ (Bottom/Top)	J_{sc} (mA/cm^2)	V_{oc} (V)	FF	PCE (%)	R_{ct} (Ω)	R_{rec} (Ω)	τ_e (ms)
Separated sensitization (single dye)	N719/N719	15.97 ± 0.22	0.67 ± 0.01	0.66 ± 0.01	7.06 ± 0.26	27.57 ± 1.67	13.51 ± 0.31	7.21 ± 2.16
	N749/N749	14.69 ± 0.58	0.64 ± 0.01	0.66 ± 0.01	6.21 ± 0.68	29.31 ± 0.96	15.46 ± 0.84	6.75 ± 2.34
	C106/C106	17.01 ± 0.33	0.67 ± 0.01	0.66 ± 0.01	7.52 ± 0.20	23.91 ± 2.11	10.65 ± 0.67	11.54 ± 2.01
Separated sensitization (double dyes)	N719/N749	16.01 ± 0.61	0.71 ± 0.02	0.67 ± 0.01	7.62 ± 0.12	25.77 ± 2.32	11.76 ± 1.21	10.27 ± 1.43
	N719/C106	16.16 ± 0.22	0.70 ± 0.01	0.66 ± 0.01	7.47 ± 0.14	27.21 ± 0.64	12.39 ± 0.67	7.98 ± 2.01
	N749/N719	14.74 ± 0.91	0.63 ± 0.03	0.63 ± 0.02	5.85 ± 0.46	30.42 ± 0.91	17.86 ± 0.98	6.34 ± 1.87
	N749/C106	14.08 ± 1.15	0.64 ± 0.03	0.66 ± 0.01	5.95 ± 0.65	30.24 ± 1.10	17.31 ± 0.45	6.56 ± 1.32
	C106/N719	18.31 ± 0.26	0.67 ± 0.01	0.66 ± 0.01	8.10 ± 0.05	23.61 ± 2.45	10.46 ± 0.12	12.54 ± 1.12
	C106/N749	17.93 ± 0.47	0.67 ± 0.01	0.66 ± 0.01	7.93 ± 0.19	24.75 ± 2.11	10.77 ± 0.09	11.27 ± 1.81
Mixed sensitization (double dyes)	N719 + N749	16.18 ± 0.33	0.67 ± 0.01	0.62 ± 0.02	6.72 ± 0.15	29.28 ± 2.74	13.71 ± 1.17	6.84 ± 2.16
	N719 + C106	17.06 ± 0.29	0.67 ± 0.00	0.63 ± 0.01	7.20 ± 0.78	26.72 ± 2.89	11.79 ± 0.46	8.66 ± 0.67
	N749 + C106	16.95 ± 0.34	0.67 ± 0.01	0.63 ± 0.01	7.15 ± 0.23	26.85 ± 3.21	12.35 ± 1.32	8.12 ± 2.21

*Note: J_{sc}: short-circuit current density, V_{oc}: open-circuit voltage, FF: fill factor, PCE: power conversion efficiency, R_{ct}: charge transfer resistance across the FTO glass–TiO$_2$ interfaces and TiO$_2$ NP-based interfaces, R_{rec}: recombination resistance across TiO$_2$–dye–electrolyte interface, and τ_e: electron lifetime.
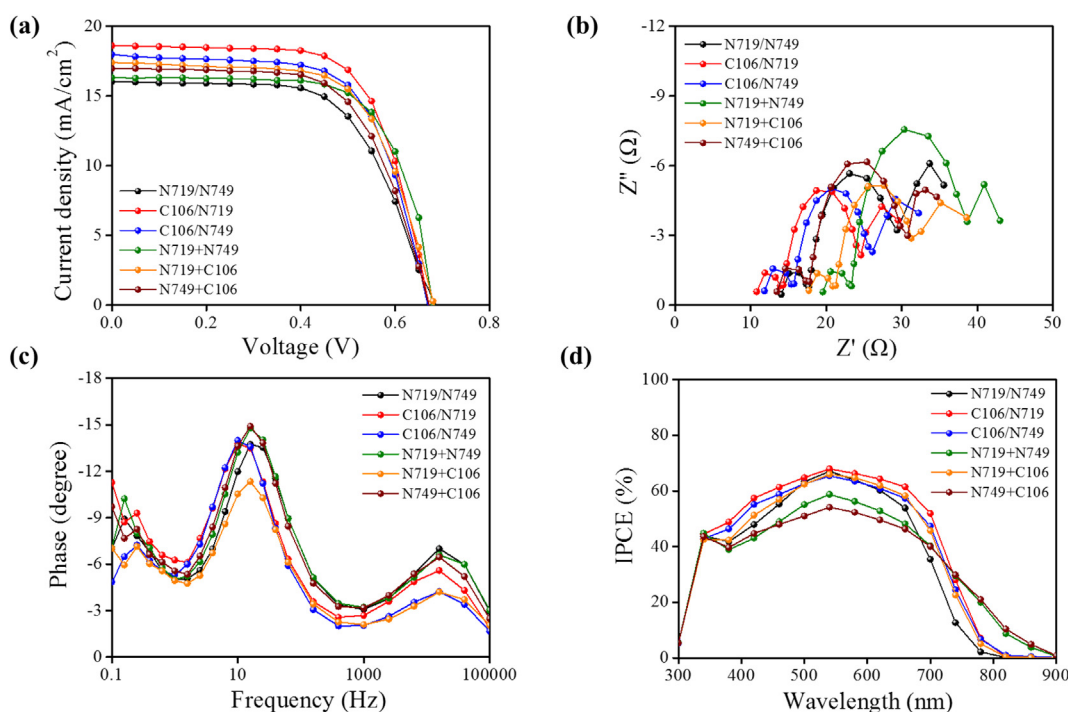

Fig. 6. (a) current–density–voltage (J–V) curves, (b) Nyquist plots, (c) Bode plots, and (d) IPCE curves concerning panchromatic DSSCs incorporated with separated and mixed sensitization using selective double dyes—N719, N749, and C106.

face, and electrolyte resistance, respectively. The separate-sensitization-based DSSCs incorporated with C106 on the bottom layer demonstrated lower R_{rec} values compared to the mixed-sensitization-based DSSCs. The resistance (R_{ct}) across the FTO glass–TiO$_2$ interfaces and TiO$_2$ NP-based interfaces can be determined using the relation $R_{total} = R_{ct}/3 + R_{rec}$, where R_{total} denotes the total DSSC resistance [29]. In this study, the separated- and mixed-sensitization-based DSSCs exhibited nearly identical R_{total} values. Fig. 6(c) depicts the Bode plots for the different panchromatic DSSCs fabricated in this study. The lifetime (τ_e) of the photogenerated electrons can be determined using the relation $\tau_e = 1/(2\pi f_{max})$, where f_{max} denotes the maximum peak frequency in the low-frequency region. As can be realized, the separated-sensitization-based DSSCs exhibit τ_e that exceed those of the mixed-sensitization DSSCs. This confirms the successful transport of electrons can be made through the separated-sensitization-based TiO$_2$ photoelectrodes. However, the photogenerated elec-

trons are combined rapidly with dyes and electrolytes when the TiO$_2$ photoelectrodes are incorporated with the mixed-sensitization. Fig. 6(d) depicts the trends concerning the incident photon–electron conversion efficiency (IPCE) observed for the different panchromatic DSSCs. As can be seen, the separated-sensitization-based DSSCs demonstrate high IPCE values in the order C106/N719 > C106/N749 > N719/N749, which far exceed the corresponding IPCE values of the mixed-sensitization-based DSSCs. This suggests that the IPCE value of panchromatic DSSCs can be improved via controlled sensitization of multiple dyes with specific light absorbance characteristics in separated TiO$_2$ TFs-based photoelectrodes.

The above results predominantly reveal that the mixed-sensitization-based panchromatic DSSCs fabricated in this study exhibit inferior photovoltaic performance compared to the separated-sensitization-based counterparts. This can be attributed to the occurrence of adverse effects in the mixed dyes. Fig. 7
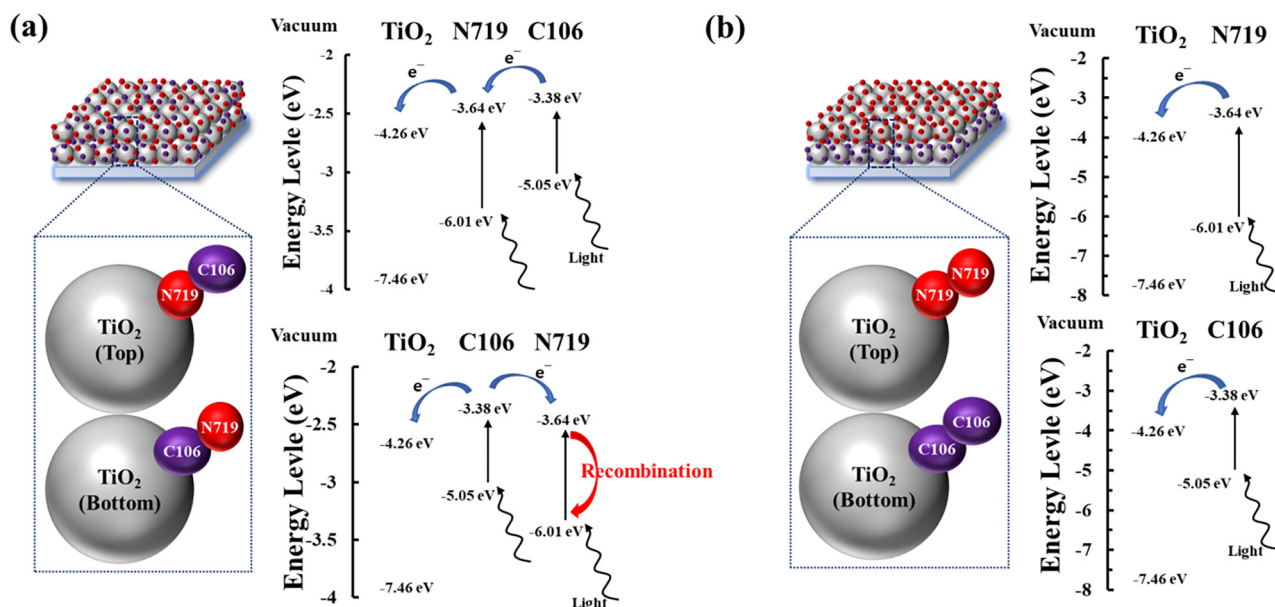
Fig. 7. Schematic of electron transport steps in bilayered TiO$_2$ TFs with (a) the mixed sensitization of N719 and C106 dyes (i.e., N719 + C106) and (b) the separated sensitization of C106 and N719 dyes (i.e., C106(bottom)/N719(top)).

depicts the possible electron-transfer routes between the C106 and N719 dyes considered as an example. It is observed that the C106 dye is characterized by a higher value of the lowest unoccupied molecular orbital (LUMO) energy level (-3.38 eV) compared to N719 (-3.64 eV). The case of mixed C106 + N719 dyes in the top layer can have an efficient electron transfer, while the case of mixed C106 + N719 dyes in the bottom layer can have a higher possibility of electron recombination (Fig. 7(a)). Therefore, the mixed C106 + N719 dye exhibits a deteriorating electron-transport behavior, which lowers the resulting current density. However, when the same dyes are sensitized separately on bilayered TiO$_2$ TFs (i.e., C106/N719), the photogenerated electrons are efficiently transported, and the panchromatic DSSC performance is maximized (Fig. 7(b)).

transport between the dyes. Therefore, it is suggested that the top and bottom layers of panchromatic DSSCs must be fabricated by incorporating TiO$_2$ TFs with low- and high-light-absorbance separately-sensitized dyes, respectively. This strategy would facilitate the efficient harvesting of the incident irradiation energy by panchromatic DSSCs.

Declaration of Competing Interest

The authors declare that they have no known competing financial interests or personal relationships that could have appeared to influence the work reported in this paper.

Conclusions

In this study, we fabricated freestanding and fixed bilayered TiO$_2$ TFs, which were separately coated with double dyes selected from N719, N749, and C106, thereby facilitating the assembly of panchromatic-DSSC photoelectrodes. The fixed TiO$_2$ TF as a bottom layer was fabricated on the surface of FTO glass via screen-printing process. Meanwhile, the freestanding TiO$_2$ TF (i.e., top layer) was fabricated using the photoresist-based sacrificing layer process. The effect of the type and location of the dye sensitization in the bilayered TiO$_2$ TFs-based photoelectrodes on DSSC performance has been systematically examined in this study. The light absorbances of the three Ru(II)-based dyes considered in this study are in the order C106 > N719 > N749 while those of their combinations (N719 + N749, C106 + N719, and C106 + N749) are much lower in comparison. The results of the different analysis performed in this study reveal that the panchromatic DSSC incorporating the separated-sensitization of C106 (bottom) and N719 (top) layers demonstrates the best performance (PCE = 8.10 %). The corresponding poorest performance is exhibited by the DSSC incorporating the separated-sensitization of N749 (bottom) and N719 (top) layers (PCE = 5.85 %). In comparison, the DSSCs incorporating bilayered TiO$_2$ TFs with mixed-sensitization of double dyes demonstrated much lower performance owing to ineffective electron

References

[1] J. Gong, K. Sumathya, Q. Qiaob, Z. Zhou, Renew. Sustain. Energy Rev. 68 (2017) 234–246.
[2] B. O'Regan, M. Grätzel, Nature 353 (1991) 737.
[3] M. Grätzel, Nature 414 (6861) (2001) 338–344.
[4] N. Tomar, A. Agrawal, V.S. Dhaka, P.K. Surolia, Sol. Energy 207 (2020) 59–76.
[5] J. Wu, Z. Lan, J. Lin, M. Huang, Y. Huang, L. Fan, et al., Chem. Rev. 115 (2015) 2136–2173.
[6] Y. Bai, F.D. Iván Mora-Seró, J. Angelis, P.W. Bisquert, Chem. Rev. 114 (2014) 10095–10130.
[7] S. Bose, V. Soni, K.R. Genwa, Int J. Sci. Res. 5 (2015) 4.
[8] A. Carella, F. Borbone, R. Centore, Front. Chem. 6 (2018) 481.
[9] Y. Li, L. Ma, Y. Yoo, G. Wang, X. Zhang, M.J. Ko, J. Ind. Eng. Chem. 73 (2019) 351–356.
[10] M. Kokkonen, P. Talebi, J. Zhou, S. Asgari, S.A. Soomro, F. Elsehrawy, et al., J. Mater. Chem. A 9 (17) (2021) 10527–10545.
[11] R.K. Chitumalla, J. Jang, Bull. Korean Chem. Soc. 38 (10) (2017) 1209–1213.
[12] J. Oh, W. Ghanna, H. Kang, F. Nesbitt, S. Providence, J. Uddina, Inorganica Chimica. Acta. 482 (2018) 935–943.

[13] G.C. Vougioukalakis, A.I. Philippopoulos, T. Stergiopoulos, P. Falaras, Coord. Chem. Rev. 255 (21-22) (2011) 2602–2621.

[14] A. Islam, T.H. Chowdhury, C. Qin, L. Han, J.-J. Lee, I. Bedja, et al., Sustain Energy Fuels 2 (1) (2018) 209–214.

[15] H.L. Cha, S. Seok, H.J. Kim, S. Thogiti, B.S. Goud, G. Shin, et al., J. Ind. Eng. Chem. 99 (2021) 117–125.

[16] S.P. Singh, M. Chandrasekharam, K.S.V. Gupta, A. Islam, L. Han, G.D. Sharma, Org. Electron. 14 (2013) 1237–1241.

[17] G. Koyyada, R.K. Chitumalla, S. Thogiti, J.H. Kim, J. Jang, M. Chandrasekharam, et al., Molecules 24 (19) (2019) 3554.

[18] G. Koyyada, S. Shome, M. Chandrasekharam, G.D. Sharmac, S.P. Singh, RSC Adv. 6 (2016) 41151.

[19] Z. Zolkepli, A. Lim, P. Ekanayake, K. Tennakoon, J. Biophys. 2015 (2015) 8.

[20] L.N.D. Quang, A.K. Kaliamurthy, N.H. Hao, Optical Mat. 111 (2021) 0925–3467.

[21] K. Lee, S.W. Park, M.J. Ko, K. Kim, N.-G. Park, Nat. Mater. 8 (8) (2009) 665–671.

[22] J.-J. Cid, J.-H. Yum, S.-R. Jang, M. Nazeeruddin, E. Martínez-Ferrero, E. Palomares, et al., Angew. Chem. 46 (44) (2007) 8358–8362.

[23] Y. Masatoshi, O.K. Nobuko, K. Mitsuhiko, S. Kazuhiro, S. Hideki, Sol. Energy Mater. Sol. Cells 94 (2) (2010) 297–302.

[24] A. Guinier, X-ray diffraction, Freeman, San Francisco, 1963, p. 124.

[25] R.A. Spurr, H. Myers, Analytical Chem. 29 (1957) 760–762.

[26] C. Kreitner, E. Erdmann, W.W. Seidel, K. Heinze, Inorg. Chem. 54 (23) (2015) 11088–11104.

[27] A.O. Adeloye, P.A. Ajibade, J Spectrosc. 2014 (2014) 1–10.

[28] P. Wen, Y. Han, W. Zhao, Int. J. Photoenergy 2012 (2012) 7.

[29] R. Kern, R. Sastrawan, J. Ferber, R. Stangl, J. Luther, Electrochim Acta. 47 (26) (2002) 4213–4225.